On Valence-Band Splitting in Layered MoS_2

Youwei Zhang,[†,‡] Hui Li,[†] Haomin Wang,[‡] Ran Liu,[*,†] Shi-Li Zhang,[*,§] and Zhi-Jun Qiu[*,†]

[†]State Key Laboratory of ASIC & System, School of Information Science and Technology, Fudan University, Shanghai 200433, China, [‡]State Key Laboratory of Functional Materials for Informatics, Shanghai Institute of Microsystem & Information Technology, Chinese Academy of Sciences, Changning Road 865, Shanghai 200050, China, and [§]Solid-State Electronics, The Ångström Laboratory, Uppsala University, Box 534, Uppsala SE-751 21, Sweden

ABSTRACT As a representative two-dimensional semiconducting transition-metal dichalcogenide (TMD), the electronic structure in layered MoS_2 is a collective result of quantum confinement, interlayer interaction, and crystal symmetry. A prominent energy splitting in the valence band gives rise to many intriguing electronic, optical, and magnetic phenomena. Despite numerous studies, an experimental determination of valence-band splitting in few-layer MoS_2 is still lacking. Here, we show how the valence-band maximum (VBM) splits for one to five layers of MoS_2. Interlayer coupling is found to contribute significantly to phonon energy but weakly to VBM splitting in bilayers, due to a small interlayer hopping energy for holes. Hence, spin–orbit coupling is still predominant in the splitting. A temperature-independent VBM splitting, known for single-layer MoS_2, is, thus, observed for bilayers. However, a Bose–Einstein type of temperature dependence of VBM splitting prevails in three to five layers of MoS_2. In such few-layer MoS_2, interlayer coupling is enhanced with a reduced interlayer distance, but thermal expansion upon temperature increase tends to decouple adjacent layers and therefore decreases the splitting energy. Our findings that shed light on the distinctive behaviors about VBM splitting in layered MoS_2 may apply to other hexagonal TMDs as well. They will also be helpful in extending our understanding of the TMD electronic structure for potential applications in electronics and optoelectronics.

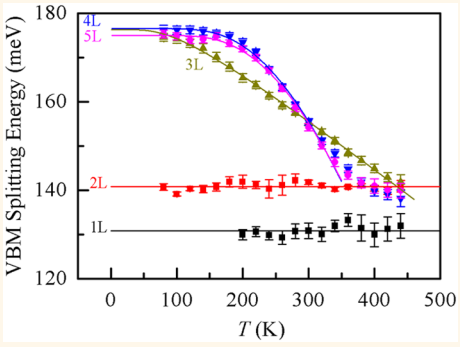

KEYWORDS: molybdenum disulfide · valence-band splitting · spin–orbit coupling · interlayer coupling · photoluminescence spectroscopy

Layered transition-metal dichalcogenides (TMDs) have lately attracted considerable attention due to their exotic electronic and optical properties.[1,2] One of intriguing features is the possibility to control quantum degrees of freedom such as electron spin, valley pseudospin, and layer pseudospin.[3] Unlike graphene, TMDs have a strong spin–orbit coupling (SOC) originating from the d orbitals of the heavy transition-metal atoms.[4] This remarkable SOC combined with the unique crystal symmetry leads to coupling of spin and valley degrees of freedom.[5−7] In semiconducting TMDs, the valley index represents an additional dimension, to charge and spin, that can be exploited in information processing. This extra dimension is derived from the confinement of holes in distinct valence band maxima (VBMs) each with a given energy level but at different positions in the momentum space. Exploitation of such interesting features can lead to potential spintronic and valleytronic devices.

In monolayer hexagonal TMDs, such as MoS_2, the SOC lifts the spin degeneracy of the energy bands due to breaking of the inversion symmetry.[8] This effect is particularly pronounced in the valence band, giving rise to a sizable spin splitting (>0.1 eV) of the valence-band edge at the K point of the Brillouin zone.[9] This splitting makes it desirable for the observation of many physical phenomena such as the spin-Hall effect,[10] valley-Hall effect,[11] and optical circular dichroism.[12] In few-layer TMDs, interlayer van der Waals interactions, besides SOC, play a non-negligible role in determining VBM splitting.[13] Recent theoretical calculations show that the interlayer distance has strong effects on the VBM splitting.[14] Decreasing the interlayer separation would lead to strengthening of the interlayer coupling, a hypothesis that can be verified using few-layer MoS_2.

The VBM splitting in monolayer MoS_2 caused by the spin–orbit coupling has been fully characterized.[15,16] In view of the

* Address correspondence to rliu@fudan.edu.cn, shili.zhang@angstrom.uu.se, zjqiu@fudan.edu.cn.

Received for review June 10, 2015 and accepted July 29, 2015.

Published online July 29, 2015
10.1021/acsnano.5b03505

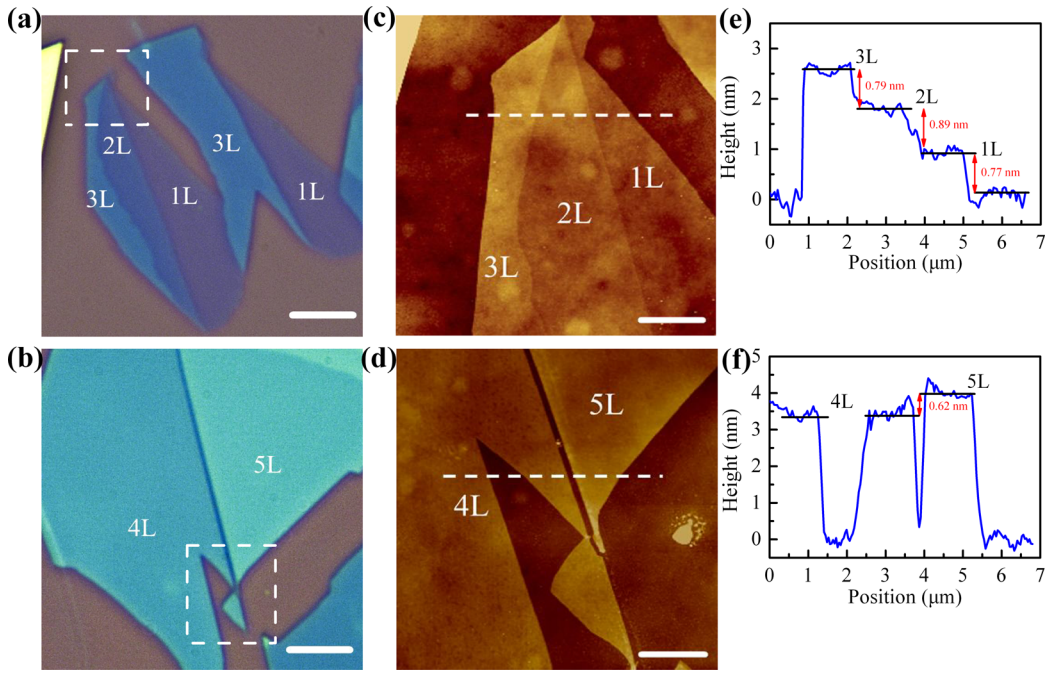

Figure 1. Optical and AFM images of MoS_2 flakes. (a, b) Optical images of 1L, 2L, 3L and 4L, 5L MoS_2 on SiO_2/Si substrate, respectively. The scale bars are both 5 μm. (c, d) AFM images of the white dashed squares in (a) and (b). The scale bars are both 2 μm. (e and f) Height profiles along the dashed lines in (c) and (d), respectively.

change in the conduction band leading to a fundamental transition from direct to indirect bandgap when the number of layers is increased from one to a few,[9,17] it is highly desirable to explore how the splitting would evolve with increasing number of layers in MoS_2. This is what we intend to systematically investigate in the present work using temperature-dependent photoluminescence (PL) spectroscopy, a technique capable of effectively probing the electronic and structural properties of nanomaterials.[18] Bandgap determination using PL spectroscopy is in general inaccurate and can differ from the electronic bandgap due to large exciton binding energies in two-dimensional materials (0.5−1 eV, theoretical calculations).[19−23] However, the VBM splitting deduced from the energy difference between excitonic peaks A and B is less affected, because the difference in binding energy between the excitons is negligibly small at ~10 meV.[24]

RESULTS AND DISCUSSION

Atomically thin MoS_2 flakes were mechanically exfoliated from bulk crystals onto a heavily doped silicon substrate capped with a 300 nm thick thermal grown SiO_2 film. The number of layers was identified using optical microscopy, atomic force microscopy (AFM), and Raman spectroscopy. The sample preparation and characterization are detailed in the Methods. Figure 1a,b shows the optical images of thin MoS_2 flakes consisting of monolayer (1L), bilayer (2L), trilayer (3L), tetralayer (4L), and pentalayer (5L) MoS_2 sheets. It is seen that the optical contrast of MoS_2 increases with the number of atomic layers.[25] As such, single- and few-layer MoS_2 films show distinctive optical contrast against the substrate in Figure 1. This identification was confirmed using AFM; see Figure 1c,d for AFM topography images taken from the regions marked by the dashed squares in Figure 1a,b, respectively. The number of layers was determined by height measurement with respect to the SiO_2 surface from the line profiles in the AFM images. The transition from SiO_2 to MoS_2 toward the right in Figure 1e gives a thickness of 0.77 nm, which is compatible with the thickness of 1L MoS_2. It should be noted that 1L MoS_2 flakes measured on SiO_2 show a widespread in thickness from 0.6 to 1.2 nm in the literature.[26−29] This reflects the difficulty in accurately determining the thickness of 1L MoS_2, likely due to the presence of adsorbates between the flake and the substrate[27] or to the difference in deflection force the AFM tip experiences between the flake and the substrate.[30] Therefore, measuring the height between two adjacent layers of the same MoS_2 flake is obviously advantageous. Our measurements in Figure 1e,f yield 0.89 nm between 2L and 1L (second layer), 0.79 nm between 3L and 2L (third layer), and 0.62 nm between 5L and 4L (fifth layer), *i.e.*, a clear decreasing trend for increasing numbers of layers. This is consistent with the theoretical expectation that thicker MoS_2 layers have a smaller interlayer spacing.[14,31] Furthermore, the interlayer distance for the fifth layer is in good agreement with the theoretical interlayer spacing of 6.15 Å in bulk MoS_2.[32] The nanoflakes were also characterized using Raman spectroscopy, which gave supporting results in Figure S1 (Supporting Information) with decreasing frequency of the in-plane vibration E_{2g}^1 and increasing

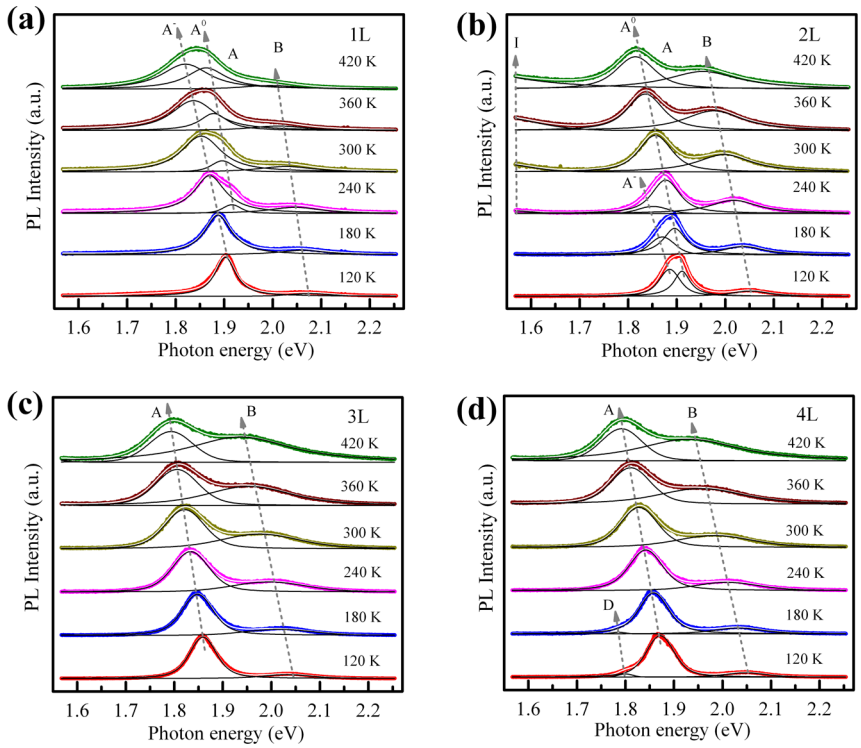

Figure 2. PL characterization of MoS_2 flakes at different temperatures. PL spectra of 1L (a), 2L (b), 3L (c), and 4L (d) MoS_2. The Gaussian components fitting to the PL spectra are shown as the thin, black lines, while the thin, white lines embedded in the thick, colored lines (representing the experimental data) are the fitting results. A^0 (or A in 3L and 4L) and B represent the two exciton emissions while A^- in 1L and 2L indicates the trion emission. I in (b) accounts for the indirect emission and D in (d) the defect-assisted emission.

frequency of the out-of-plane vibration A_{1g} with increasing number of MoS_2 layer. This opposite behavior of $E_{2g}{}^1$ and A_{1g} leads to an increase in frequency difference from 18.8 cm^{-1} in 1L to 24.6 cm^{-1} in 5L.

The quantum confinement effect causes the electronic structure of MoS_2 to transform from indirect to direct gap semiconductor as the material is exfoliated down to a monolayer in thickness.[9] The two PL emission peaks around 1.90 and 2.05 eV in Figure 2a are characteristic of 1L MoS_2. They correspond to the direct excitonic transitions A and B between the minimum of the conduction band and the maxima of split valence band at the K point.[17] Although few-layer MoS_2 are an indirect bandgap semiconductor, its PL continues to be dominated by peaks A and B in 2L to 5L MoS_2; cf. Figure 2b–d and Figure S2 (Supporting Information). This originates from the direct-gap hot luminescence,[9] which is different from the indirect bandgap semiconductor silicon with an almost total PL quenching.

The broad peak A in the PL spectra of the 1L and 2L MoS_2 comprises two components, A^0 and A^-. The two-dimensionality in atomically thin MoS_2 enhances the Coulomb interaction because of reduced dielectric screening, large carrier effective masses, and strong quantum confinement, all favoring the formation of tightly bound excitons. Once a small number of excess electrons are present, they can capture the photoexcited excitons to form trions, which represent a bound state of two electrons and a hole.[33] The higher energy emission in complex A is the neutral exciton, A^0, while the lower energy peak is a trion, A^-. Their energy difference defines the trion binding energy: 43 meV in 1L and 25 meV in 2L (Figure S3, Supporting Information). The trion PL peak is difficult to resolve in flakes with 3L or more. In addition, the PL peak I emerging at 1.59 eV in the 2L MoS_2 is attributed to the transition across the indirect bandgap between the Γ and K points.[34] The PL peak D at 1.8 eV in the 4L and 5L MoS_2 originates from defect-bound neutral excitons.[35]

The peak positions of both excitons A and B in all layered MoS_2 nanoflakes show red-shift with increasing temperature. The shift is caused by the temperature dependence of the semiconductor bandgap. In order to quantify the exciton peak shift, depicted in Figure S5 (Supporting Information), the following semiempirical bandgap expression[36] is employed

$$E(T) = E_0 - S\langle\hbar\omega\rangle\left[\coth\left(\frac{\langle\hbar\omega\rangle}{2k_BT}\right) - 1\right] \quad (1)$$

where E_0 is the transition energy at 0 K and S is the Huang–Rhys factor that represents the strength of the exciton–phonon coupling; a higher Huang–Rhys factor indicates stronger coupling. $\langle\hbar\omega\rangle$ is the average phonon energy and k_B is the Boltzmann constant. The extracted $\langle\hbar\omega\rangle$ and S for A and B are shown in Figure 3. The difference in $\langle\hbar\omega\rangle$ between A and B is insignificant,

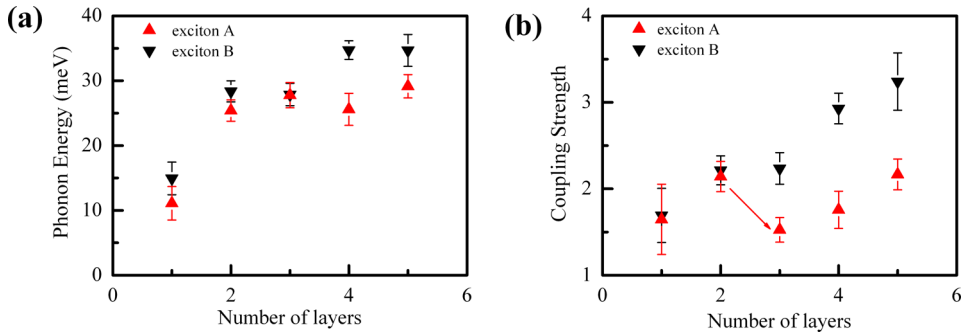

Figure 3. Phonon energy and exciton−phonon coupling strength in MoS_2. (a) Layer dependence of average energy for phonon interacting with excitons A and B. (b) Layer dependence of the strength of phonon coupling with excitons A and B. The red arrow indicates a sudden drop of the coupling strength for exciton A when moving from 2L to 3L. Error bars are determined from the standard deviations incurred in the curve fitting of the experimental data in Figure S5 with eq 1.

but a sudden jump from ~12 meV for 1L to ~25 meV for 2L is observed. Thereafter, the increase is minor between 2L and 5L. This behavior is similar to the shift of the out-of-plane vibration A_{1g} with the number of MoS_2 layers determined by means of Raman spectroscopy (Figure S1, Supporting Information). In comparison with 1L, the interlayer coupling in 2L significantly strengthens the atom−atom interaction in the vertical direction. However, the interlayer coupling has apparently different effects on the coupling strength of excitons A and B with phonons. The coupling strength for exciton B increases, expectedly, monotonically from 1.5 to 3 with increasing number of layers. However, the coupling strength for exciton A drops from 2 to 1.5 unexpectedly when the number of layers is increased from 2L to 3L. It then continues to increase after 3L as for exciton B. This development of the coupling strength for exciton A is poorly understood. Likely changes in the electronic structure of the split valence bands in 3L and above need be scrutinized. The difference in phonon coupling factors between excitons A and B in thick MoS_2 is likely related to their distinct effective masses. It has been shown that exciton B has a larger effective mass than exciton A in thicker MoS_2[37] and a larger exciton effective mass causes a stronger exciton−phonon coupling.[38]

The energy difference between excitons A and B defines the VBM splitting at the K point. The temperature behavior of the VBM splitting for all the MoS_2 nanoflakes is shown in Figure 4. The splitting energies for 1L and 2L are both independent of temperature. In 1L, the VBM splitting is entirely due to the strong SOC leading to spin-split bands. The SOC is a relativistic effect mostly determined by the inner orbits of an atom and represents therefore an atomic property.[39] Hence, the VBM splitting energy in 1L is insensitive to the temperature variation. Unlike 1L MoS_2 with a structural inversion asymmetry, its 2L counterpart, stacked in the Bernal configuration, possesses both time-reversal and inversion symmetries. As a result, it splits to the degenerate spin-up and spin-down bands.[40] The VBM splitting thus arises from a combined effect of SOC and

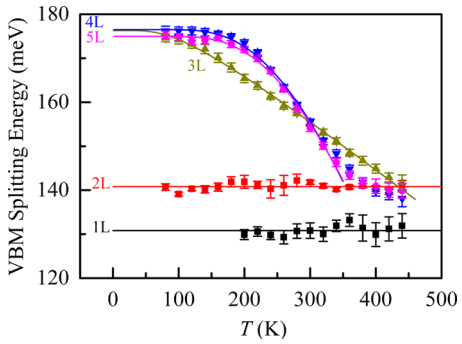

Figure 4. Temperature dependence of VBM splitting in MoS_2. VBM splitting energies for MoS_2 with layers from 1L to 5L as a function of temperature. Solid lines are the fitting results according to eq 2. Error bars are determined from the standard deviations incurred in the curve fitting of the PL spectra of MoS_2 with a Gaussian function.

interlayer coupling. The splitting energy increases from 130 meV in 1L to 140 meV in 2L. However, it has been recently reported that the interlayer hopping energy for holes is smaller than the spin splitting energy due to a large layer separation in 2L MoS_2.[3,41,42] Consequently, the interlayer hole hopping, *i.e.*, holes consecutively hopping between neighboring layers, is virtually suppressed. The mixture of the wave function of the holes in different layers is negligible, and thus, the 2L MoS_2 can be treated as two separated 1L. This explains the small difference in VBM splitting between 1L and 2L in terms of both energy and temperature behavior. The interlayer scattering, which is an effective relaxation mechanism for few-layer Bernal stackings,[7] is significantly suppressed, and thus the hole mobility in 2L is expectedly identical to that of 1L MoS_2.

The interlayer hopping amplitude can be tuned by varying the interlayer distance.[7] Reducing the layer separation, by increasing number of layers, can improve the interlayer hopping and coupling,[43] which is indeed observed in Figure 4 with VBM splitting energies around 175 meV for 3L to 5L below 100 K. At high temperatures, the VBM splitting energy approaches that of 2L. Thermal expansion can effectively decouple adjacent layers by increasing interlayer spacing and reducing interlayer interaction and scattering.

At sufficiently high temperatures, the coupling between layers becomes so weak that they behave as isolated single layers. The temperature dependence of the VBM splitting in 3L to 5L in a fairly large temperature interval can be approximately described using a Bose−Einstein type of expression[44]

$$E_{B-A}(T) = E_{B-A}(0) - \frac{\alpha}{\exp\left(\frac{\Theta}{k_B T}\right) - 1} \quad (2)$$

where $E_{B-A}(0)$ is the VBM splitting energy at 0 K and α and Θ are fitting parameters. Curve fitting in Figure 4 yields α equal to zero for both 1L and 2L (in which interlayer hopping is totally quenched) ,32 meV for 3L, and 556 meV for both 4L and 5L. This trend with an increasing α is consistent with the behavior of interlayer coupling with increasing number of layers. Thus, α can be correlated to the interlayer coupling strength. Along this line, an enhanced interlayer coupling leads to an increased Θ from 24 meV for 3 L to 85−87 meV for 4L−5L. It has been established that the out-of-plane vibration represented by A_{1g} stiffens with increasing number of layers. Hence, Θ in eq 2 can be correlated to the out-of-plane transverse optical (TO) phonon energy. However, it should be mentioned that this simplified Bose−Einstein model, assuming a temperature-independent α, may overestimate the interlayer hopping strength and phonon energy and result in appreciable deviations from experimental data especially at high temperatures.

CONCLUSION

In this work, we have carried out an extensive investigation in order to experimentally determine the VBM splitting in single- and few-layer MoS_2. Specifically, we have systematically investigated the VBM splitting using PL spectroscopy operated at different temperatures. The temperature dependency of excitons A and B in all samples studied can be well described by a semiempirical relation incorporating average phonon energy and exciton−phonon coupling strength as two key parameters. The phonon energy is found to be enhanced with the addition of extra layers due to increased interlayer coupling. However, the interlayer coupling only has a weak contribution to the VBM splitting energy for 2L MoS_2, due to a small interlayer hopping energy for holes, and it behaves as if they were two independent monolayers. As a result, the spin−orbit coupling dominates the VBM splitting in both 1L and 2L whose VBM splitting energy exhibits a temperature-independent behavior. For thicker layers 3L to 5L, the layer separation is reduced, owing to a stronger interlayer coupling, and a larger VBM splitting is obtained. However, this remarkably increased VBM splitting energy decreases monotonically with increasing temperature following a Bose−Einstein-like behavior in a fairly large temperature interval. This decrease is attributed to thermal expansion that weakens the interlayer coupling. In the extreme when the interlayer coupling becomes negligible, the VBM splitting energy asymptotically approaches that of 2L MoS_2. The observed distinctive VBM splitting behaviors in single- to few-layer MoS_2 may also apply to other hexagonal TMDs. This study can extend our understanding of the TMD electronic structure for potential applications in electronics and optoelectronics.

METHODS

Thin MoS_2 flakes were peeled off from bulk MoS_2 (SPI supplies) by mechanical exfoliation. They were subsequently transferred to a heavily doped *p*-type Si substrate with a 300 nm thick thermally grown SiO_2. The transferred MoS_2 flakes were identified using an optical microscope (Keyence digital microscope VHX-600). The thickness of the flakes was measured using AFM (Dimension 3100 with Nanoscope IIIa controller, Veeco) operated in tapping mode under ambient conditions. Raman and PL spectra were acquired using confocal micro-Raman spectroscopy (Renishaw inVia) in a backscattering configuration with an Ar ion laser at 514.5 nm. The backscattered light was collected through a 100× objective and dispersed by a grating of 1800 lines/mm with a spectral resolution of ~1.0 cm^{-1} and a peak position accuracy of 0.1 cm^{-1}. The power of the excitation laser line was kept well below 0.1 mW in order to avoid sample heating.

Conflict of Interest: The authors declare no competing financial interest.

Acknowledgment. This work is partially supported by the Special Funds for Major State Basic Research Projects of China (No. 2011CBA00603), the National Natural Science Foundation of China (Nos. 61204090 and 61171010), the Shanghai Municipal Natural Science Foundation (No. 12ZR1402700), the Fundamental Research Project of Young Teachers to Enhance Research Capacity, Fudan University (No. 20520133248), the State Key Laboratory of ASIC & System, Fudan University (No. 2015MS005), the Knut and Alice Wallenberg Foundation (No. 2011.0082), and the Swedish Research Council (No. 2014-5591).

Supporting Information Available: The Supporting Information is available free of charge on the ACS Publications website at DOI: 10.1021/acsnano.5b03505.

Raman characterization of MoS_2 flakes, PL spectra for 5L MoS_2, trion binding energy in MoS_2, calculation of electron density in 1L MoS_2, and temperature dependence of exciton energies in MoS_2 (PDF)

REFERENCES AND NOTES

1. Wang, Q. H.; Kalantar-Zadeh, K.; Kis, A.; Coleman, J. N.; Strano, M. S. Electronics and Optoelectronics of Two-Dimensional Transition Metal Dichalcogenides. *Nat. Nanotechnol.* **2012**, *7*, 699–712.
2. Xia, F.; Wang, H.; Xiao, D.; Dubey, M.; Ramasubramaniam, A. Two-Dimensional Material Nanophotonics. *Nat. Photonics* **2014**, *8*, 899–907.
3. Xu, X.; Yao, W.; Xiao, D.; Heinz, T. F. Spin and Pseudospins in Layered Transition Metal Dichalcogenides. *Nat. Phys.* **2014**, *10*, 343–350.
4. Mattheiss, L. F. Band Structures of Transition-Metal-Dichalcogenide Layer Compounds. *Phys. Rev. B* **1973**, *8*, 3719–3740.

5. Xiao, D.; Liu, G.-B.; Feng, W.; Xu, X.; Yao, W. Coupled Spin and Valley Physics in Monolayers of MoS_2 and Other Group-VI Dichalcogenides. *Phys. Rev. Lett.* **2012**, *108*, 196802.
6. Zeng, H.; Dai, J.; Yao, W.; Xiao, D.; Cui, X. Valley Polarization in MoS_2 Monolayers by Optical Pumping. *Nat. Nanotechnol.* **2012**, *7*, 490–493.
7. Suzuki, R.; Sakano, M.; Zhang, Y. J.; Akashi, R.; Morikawa, D.; Harasawa, A.; Yaji, K.; Kuroda, K.; Miyamoto, K.; Okuda, T.; et al. Valley-Dependent Spin Polarization in Bulk MoS_2 with Broken Inversion Symmetry. *Nat. Nanotechnol.* **2014**, *9*, 611–617.
8. Zhu, Z. Y.; Cheng, Y. C.; Schwingenschlögl, U. Giant Spin-Orbit-Induced Spin Splitting in Two-Dimensional Transition-Metal Dichalcogenide Semiconductors. *Phys. Rev. B: Condens. Matter Mater. Phys.* **2011**, *84*, 153402.
9. Mak, K. F.; Lee, C.; Hone, J.; Shan, J.; Heinz, T. F. Atomically Thin MoS_2: a New Direct-Gap Semiconductor. *Phys. Rev. Lett.* **2010**, *105*, 136805.
10. Wunderlich, J.; Kaestner, B.; Sinova, J.; Jungwirth, T. Experimental Observation of the Spin-Hall Effect in a Two-Dimensional Spin-Orbit Coupled Semiconductor System. *Phys. Rev. Lett.* **2005**, *94*, 047204.
11. Mak, K. F.; McGill, K. L.; Park, J.; McEuen, P. L. The Valley Hall Effect in MoS_2 Transistors. *Science* **2014**, *344*, 1489–1492.
12. Cao, T.; Wang, G.; Han, W.; Ye, H.; Zhu, C.; Shi, J.; Niu, Q.; Tan, P.; Wang, E.; Liu, B.; et al. Valley-Selective Circular Dichroism of Monolayer Molybdenum Disulphide. *Nat. Commun.* **2012**, *3*, 887.
13. Han, S. W.; Kwon, H.; Kim, S. K.; Ryu, S.; Yun, W. S.; Kim, D. H.; Hwang, J. H.; Kang, J.-S.; Baik, J.; Shin, H. J.; et al. Band-Gap Transition Induced by Interlayer van der Waals Interaction in MoS_2. *Phys. Rev. B: Condens. Matter Mater. Phys.* **2011**, *84*, 045409.
14. Xiao, J.; Long, M.; Li, X.; Zhang, Q.; Xu, H.; Chan, K. S. Effects of van der Waals Interaction and Electric Field on the Electronic Structure of Bilayer MoS_2. *J. Phys.: Condens. Matter* **2014**, *26*, 405302.
15. Sun, L.; Yan, J.; Zhan, D.; Liu, L.; Hu, H.; Li, H.; Tay, B. K.; Kuo, J.-L.; Huang, C.-C.; Hewak, D. W.; et al. Spin-Orbit Splitting in Single-Layer MoS_2 Revealed by Triply Resonant Raman Scattering. *Phys. Rev. Lett.* **2013**, *111*, 126801.
16. Alidoust, N.; Bian, G.; Xu, S.-Y.; Sankar, R.; Neupane, M.; Liu, C.; Belopolski, I.; Qu, D.-X.; Denlinger, J. D.; Chou, F.-C.; et al. Observation of Monolayer Valence Band Spin-Orbit Effect and Induced Quantum Well States in MoX_2. *Nat. Commun.* **2014**, *5*, 4673.
17. Splendiani, A.; Sun, L.; Zhang, Y.; Li, T.; Kim, J.; Chim, C.-Y.; Galli, G.; Wang, F. Emerging Photoluminescence in Monolayer MoS_2. *Nano Lett.* **2010**, *10*, 1271–1275.
18. Kumar, C. S. S. R. *UV-Vis and Photoluminescence Spectroscopy for Nanomaterials Characterization*. Springer: Berlin, Heidelberg, 2013.
19. Komsa, H.-P.; Krasheninnikov, A. V. Effects of Confinement and Environment on the Electronic Structure and Exciton Binding Energy of MoS_2 from First Principles. *Phys. Rev. B: Condens. Matter Mater. Phys.* **2012**, *86*, 241201.
20. Cheiwchanchamnangij, T.; Lambrecht, W. R. L. Quasiparticle Band Structure Calculation of Monolayer, Bilayer, and Bulk MoS_2. *Phys. Rev. B: Condens. Matter Mater. Phys.* **2012**, *85*, 205302.
21. Ramasubramaniam, A. Large Excitonic Effects in Monolayers of Molybdenum and Tungsten Dichalcogenides. *Phys. Rev. B: Condens. Matter Mater. Phys.* **2012**, *86*, 115409.
22. Qiu, D. Y.; da Jornada, F. H.; Louie, S. G. Optical Spectrum of MoS_2: Many-Body Effects and Diversity of Exciton States. *Phys. Rev. Lett.* **2013**, *111*, 216805.
23. Shi, H.; Pan, H.; Zhang, Y.-W.; Yakobson, B. I. Quasiparticle Band Structures and Optical Properties of Strained Monolayer MoS_2 and WS_2. *Phys. Rev. B: Condens. Matter Mater. Phys.* **2013**, *87*, 155304.
24. Berghäuser, G.; Malic, E. Analytical Approach to Excitonic Properties of MoS_2. *Phys. Rev. B: Condens. Matter Mater. Phys.* **2014**, *89*, 125309.
25. Li, H.; Wu, J.; Huang, X.; Lu, G.; Yang, J.; Lu, X.; Xiong, Q.; Zhang, H. Rapid and Reliable Thickness Identification of Two-Dimensional Nanosheets Using Optical Microscopy. *ACS Nano* **2013**, *7*, 10344–10353.
26. Radisavljevic, B.; Radenovic, A.; Brivio, J.; Giacometti, V.; Kis, A. Single-Layer MoS_2 Transistors. *Nat. Nanotechnol.* **2011**, *6*, 147–150.
27. Eda, G.; Yamaguchi, H.; Voiry, D.; Fujita, T.; Chen, M.; Chhowalla, M. Photoluminescence from Chemically Exfoliated MoS_2. *Nano Lett.* **2011**, *11*, 5111–5116.
28. Li, H.; Zhang, Q.; Yap, C. C. R.; Tay, B. K.; Edwin, T. H. T.; Olivier, A.; Baillargeat, D. From Bulk to Monolayer MoS_2: Evolution of Raman Scattering. *Adv. Funct. Mater.* **2012**, *22*, 1385–1390.
29. Buscema, M.; Barkelid, M.; Zwiller, V.; van der Zant, H. S. J.; Steele, G. A.; Castellanos-Gomez, A. Large and Tunable Photothermoelectric Effect in Single-Layer MoS_2. *Nano Lett.* **2013**, *13*, 358–363.
30. Nemes-Incze, P.; Osváth, Z.; Kamarás, K.; Biró, L. P. Anomalies in Thickness Measurements of Graphene and Few Layer Graphite Crystals by Tapping Mode Atomic Force Microscopy. *Carbon* **2008**, *46*, 1435–1442.
31. Cheng, Y.; Zhu, Z.; Schwingenschlögl, U. Role of Interlayer Coupling in Ultra Thin MoS_2. *RSC Adv.* **2012**, *2*, 7798–7802.
32. Frindt, R. F. Single Crystals of MoS_2 Several Molecular Layers Thick. *J. Appl. Phys.* **1966**, *37*, 1928–1929.
33. Mak, K. F.; He, K.; Lee, C.; Lee, G. H.; Hone, J.; Heinz, T. F.; Shan, J. Tightly Bound Trions in Monolayer MoS_2. *Nat. Mater.* **2012**, *12*, 207–211.
34. Dou, X.; Ding, K.; Jiang, D.; Sun, B. Tuning and Identification of Interband Transitions in Monolayer and Bilayer Molybdenum Disulfide Using Hydrostatic Pressure. *ACS Nano* **2014**, *8*, 7458–7464.
35. Chow, P. K.; Jacobs-Gedrim, R. B.; Gao, J.; Lu, T.-M.; Yu, B.; Terrones, H.; Koratkar, N. Defect-Induced Photoluminescence in Monolayer Semiconducting Transition Metal Dichalcogenides. *ACS Nano* **2015**, *9*, 1520–1527.
36. O'Donnell, K. P.; Chen, X. Temperature Dependence of Semiconductor Band Gaps. *Appl. Phys. Lett.* **1991**, *58*, 2924–2926.
37. Coehoorn, R.; Haas, C.; de Groot, R. A. Electronic Structure of $MoSe_2$, MoS_2, and WSe_2. II. The Nature of the Optical Band Gaps. *Phys. Rev. B: Condens. Matter Mater. Phys.* **1987**, *35*, 6203–6206.
38. Agranovich, V. M.; Antonyuk, B. P.; Ivanova, E. P.; Mal'shukov, A. G. Self-Localization of Excitons in Quasi-One-Dimensional and Quasi-Two-Dimensional Semiconductors. *Sov. Phys. JETP* **1977**, *45*, 322–327.
39. Savushkin, L. N.; Toki, H. *The Atomic Nucleus as a Relativistic System*; Springer: Berlin, Heidelberg, 2010.
40. Jiang, T.; Liu, H.; Huang, D.; Zhang, S.; Li, Y.; Gong, X.; Shen, Y.-R.; Liu, W.-T.; Wu, S. Valley and Band Structure Engineering of Folded MoS_2 Bilayers. *Nat. Nanotechnol.* **2014**, *9*, 825–829.
41. Gong, Z.; Liu, G.-B.; Yu, H.; Xiao, D.; Cui, X.; Xu, X.; Yao, W. Magnetoelectric Effects and Valley-Controlled Spin Quantum Gates in Transition Metal Dichalcogenide Bilayers. *Nat. Commun.* **2013**, *4*, 2053.
42. Jones, A. M.; Yu, H.; Ross, J. S.; Klement, P.; Ghimire, N. J.; Yan, J.; Mandrus, D. G.; Yao, W.; Xu, X. Spin-Layer Locking Effects in Optical Orientation of Exciton Spin in Bilayer WSe_2. *Nat. Phys.* **2014**, *10*, 130–134.
43. Yu, T.; Wu, M. W. Theory of Optical Excitation Spectra and Depolarization Dynamics in Bilayer WS_2 from the Viewpoint of Excimers. *Phys. Rev. B: Condens. Matter Mater. Phys.* **2014**, *90*, 035437.
44. Viña, L.; Logothetidis, S.; Cardona, M. Temperature Dependence of the Dielectric Function of Germanium. *Phys. Rev. B: Condens. Matter Mater. Phys.* **1984**, *30*, 1979–1991.